

Electronic, magnetic and ferroelectric properties of rhombohedral AgFeO₂: an *ab initio* study

Jayita Chakraborty* and Indra Dasgupta

Department of Solid State Physics, Indian Association for the Cultivation of Science, Jadavpur, Kolkata 700032, India

(Dated: February 12, 2022)

Using first principle calculations under the framework of density functional theory we have investigated the electronic structure, magnetism and ferroelectric polarization in the triangular lattice antiferromagnet AgFeO₂, and its comparison to the isostructural system CuFeO₂. Our calculations reveal that spin orbit interaction plays an important role in determining the magnetic property of AgFeO₂ and is possibly responsible for its different magnetic ground state in comparison to CuFeO₂. Calculations of ferroelectric polarization of AgFeO₂ suggest that the spontaneous polarization arises from noncollinear spin arrangement via spin-orbit coupling. Our calculations also indicate that in addition to electronic contribution, the lattice mediated contribution to the polarization are also important for AgFeO₂.

In recent times two dimensional triangular lattice antiferromagnets have attracted much attention both theoretically as well as experimentally because of the fascinating magnetic properties displayed by them due to geometric frustration.¹⁻³ In addition, some of these compounds exhibit ferroelectricity. ABO₂-type compounds with delafossite structure provide a good example of triangular lattice antiferromagnets (TLA) and present an opportunity to study the influence of geometric spin frustration in magnetic properties.^{4,5} In ABO₂ compounds, the A-site cation has completely filled *d* orbitals, (Cu⁺-3*d*¹⁰ and Ag⁺-4*d*¹⁰), while the B-site cation has partially filled *d* orbitals (Cr³⁺-3*d*³ and Fe³⁺-3*d*⁵). Examples of ABO₂ systems include CuFeO₂, AgCrO₂, CuCrO₂, AgFeO₂ etc.⁶⁻⁸ The magnetic ground state of the delafossite CuFeO₂ has ↑↑↓↓ collinear spin structure with their spins parallel to the *c* axis.⁹ It shows multistep metamagnetic phase transitions when a varied magnetic field is applied along the *c* axis. Between the applied field 7T and 13T, there exists a noncollinear phase with a modulation vector (*q*, *q*, 0) with *q* = $\frac{1}{3}$. At a magnetic field above 13T, CuFeO₂ adopts the five-sublattice magnetic structure (↑↑↑↓↓) with collinear moments along the *c* axis.^{10,11} An in-plane electric polarization is observed only in the intermediate-field (between 7T and 13T) when the system adopts proper screw type of magnetic ordering. There are three possible mechanism for electric polarization in improper multiferroics: (i) magnetostriction, (ii) spin current model¹² or inverse Dzyaloshinskii-Moriya (DM) effect, and (iii) spin-orbit coupling dependent *d*-*p* hybridization. Due to strong coupling between magnetism and ferroelectricity, the improper multiferroelectrics are very interesting to study.¹³⁻¹⁵ Arima¹⁶ showed that the electric polarization in CuFeO₂ can be explained by the third mechanism, when the proper screw type of magnetic ordering can induce ferroelectricity through the variation in the metal (Fe-3*d*)-ligand (O-*p*) hybridization with spin-orbit coupling. Other delafossites CuCrO₂ and AgCrO₂ also exhibit ferroelectricity for a particular kind of magnetic ordering.^{11,17} AgCrO₂ exhibits ferroelectric polarization

below the temperature 21 K, in which each triangular layers of Cr³⁺ ions form parallel chains with helical spiral spin order.^{6,18} The ferroelectric polarization is also observed for CuCrO₂ with a noncollinear 120° spin structure (*q* ∼ ($\frac{1}{3}$, $\frac{1}{3}$, 0)), below 23.6 K.

The triangular lattice antiferromagnet rhombohedral (3*R*) AgFeO₂ has recently been under focus after the synthesis of the high quality samples under high pressure by Tsujimoto *et al.*¹⁹ Silver ferrite crystallizes in hexagonal structure also.²⁰ 3*R*-AgFeO₂ shows interesting magnetic, thermodynamic and ferroelectric properties.^{7,19,21} 3*R*- AgFeO₂ exhibits negative Curie-Weiss temperature ($\theta_{CW} = -140$ K) indicating antiferromagnetic interactions between Fe³⁺ (3*d*⁵) ions. The system has two magneto-structural phase transitions at $T_{N1} = 15$ K and $T_{N2} = 9$ K. The magnetic structure (ICM1 phase) for $9 \text{ K} \leq T \leq 15 \text{ K}$ is a spin-density wave with incommensurate propagation vector $k = (1, q, \frac{1}{2})$ with $q = 0.384$. At temperature below 9 K, the magnetic structure (ICM2 phase) of 3*R*-AgFeO₂ turns into an elliptical cycloid with the incommensurate propagation vector $k = (-\frac{1}{2}, q, \frac{1}{2})$ with $q = 0.2026$.¹⁹ The magnetic ground state of AgFeO₂ is drastically different from the commensurate magnetic ground state of CuFeO₂, that indicates that the A-site cation plays a crucial role in magnetism. In ICM2 phase of 3*R*-AgFeO₂, the system shows ferroelectric polarization ($\sim 300 \mu\text{C}/\text{m}^2$) for the powder sample. It is suggested that polarization is possibly driven by the spin current mechanism.¹² In view of the above it is important to investigate the origin of ferroelectricity in AgFeO₂. Since by replacing the nonmagnetic A-site (Cu with Ag) the magnetic properties are drastically changed, it is also interesting to compare the electronic and magnetic properties of these two systems.

In this paper, we have employed *ab initio* density functional calculations to investigate the electronic, magnetic and ferroelectric properties of the two dimensional system AgFeO₂, where Fe³⁺ ions (3*d*⁵, $S = \frac{5}{2}$) form a triangular lattice and also compare our results with the isostructural analogue CuFeO₂. The remainder of this paper is organised as follows: in section I we have de-

scribed the crystal structure and computational details. Section II is devoted to the detailed discussion of our results on electronic structure calculations. Finally we conclude in section III.

I. CRYSTAL STRUCTURE AND COMPUTATIONAL DETAILS

The crystal structure of $3R\text{-AFeO}_2$ ($A = \text{Cu}, \text{Ag}$) shown in Fig. 1 belongs to the rhombohedral space group $R\bar{3}m$. The silver ferrite consists of triangular layers of slightly distorted edge-sharing FeO_6 octahedra. The Ag^+ ions are in between the FeO_2 plane and are in a dumbbell ($\text{O}-\text{Ag}^+-\text{O}$) coordination as shown in Fig. 1. The structural informations of AgFeO_2 and CuFeO_2 are taken from Ref. 22.

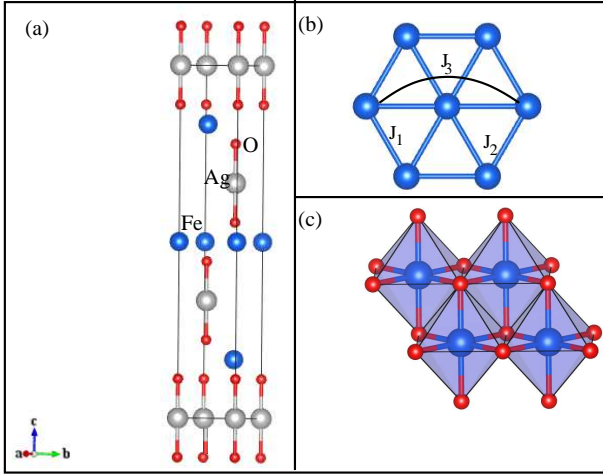


FIG. 1: (a) The unit Cell of AgFeO_2 , (b) Hexagonal ab plane, (c) Edge sharing FeO_6 octahedra.

The density-functional-theory (DFT) calculations were carried out within two different methods: (a) the plane-wave-basis-based projector augmented wave (PAW)²³ method as implemented in the Vienna *ab initio* Simulation package (VASP),²⁴ (b) the linear-muffin-tin-orbital (LMTO) basis within atomic sphere approximation (ASA) with Stuttgart TB-LMTO-ASA-47 code.²⁵ The basis set for the self-consistent electronic structure calculations for AgFeO_2 in TB-LMTO ASA includes Ag (s, p, d), Fe (s, p, d), and O (s, p) and the rest are downfolded. The density of states calculated using the TB-LMTO ASA method is found to be in good agreement with the density of states calculated using plane wave basis. We have analyzed the chemical bonding by computing the crystal orbital Hamiltonian population (COHP) as implemented in the Stuttgart tight-binding linear muffin-tin orbital (TB-LMTO) code.²⁵ The COHP provides the information regarding the specific pairs of atoms that participate in the bonding, and also the range of such interactions.

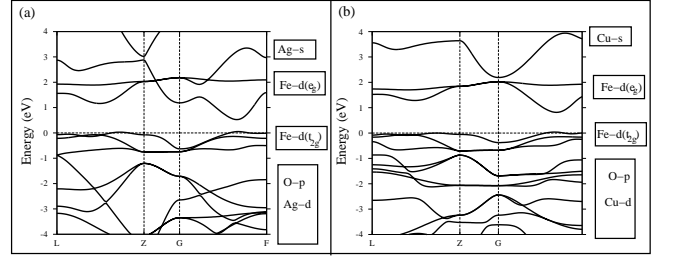


FIG. 2: LDA band structure of (a) AgFeO_2 and (b) CuFeO_2 . The zero of the energy has been set up at the LDA Fermi energy.

For plane wave based calculations, we have used a plane-wave energy cutoff of 500 eV and Γ centered k -space sampling on $(4 \times 4 \times 1)$ k -mesh. The localized Fe- d states are treated in the framework of LSDA+U method.²⁶ In order to find out the importance of spin-orbit coupling (SOC) we have also carried out the electronic structure calculation with SOC in the framework of the LSDA+U+SOC method. All structural relaxations are carried out until the Hellman-Feynman forces on each atom became less than 0.01 eV/Å. To estimate the ferroelectric polarization we have used Berry phase method²⁷ as implemented in the Vienna *ab initio* simulation package (VASP).²⁴

II. RESULTS AND DISCUSSIONS

A. Electronic and magnetic properties

1. Spin unpolarized calculation

To get insight on the electronic structure of AgFeO_2 and CuFeO_2 , we have started with spin-unpolarized calculations. The band structures calculated with the LMTO method for these systems are plotted along the various high symmetry points of the Brillouin zone of the rhombohedral lattice (see Fig. 2). The bands are plotted with respect to the Fermi energy (E_F) of the compounds. Since Fe is in $\text{Fe-}3d^5$ configuration and in an octahedral environment, the t_{2g} states, that can accommodate 6 electrons, are partially occupied, while the e_g bands are completely unoccupied. The Fe- d bands are well separated from the filled Ag- d and O- p bands for AgFeO_2 and Cu- d and O- p bands for CuFeO_2 .

The total density of states (DOS) as well as its projection onto various atomic orbitals (PDOS) are shown in Fig. 3. The DOS are projected onto Fe- d , Ag- d , and O- p orbitals for AgFeO_2 and Fe- d , Cu- d , and O- p orbitals for CuFeO_2 . The spin unpolarized calculation give rise to a metallic solution with states dominated by Fe- d character at the Fermi level (E_F) for both the systems. The Fe- d density of states are spread over -1 eV below the Fermi level to 2.0 eV above the Fermi level for both the sys-

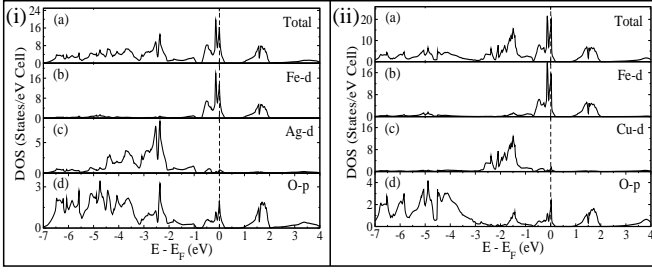


FIG. 3: Total and partial density of states (i) for

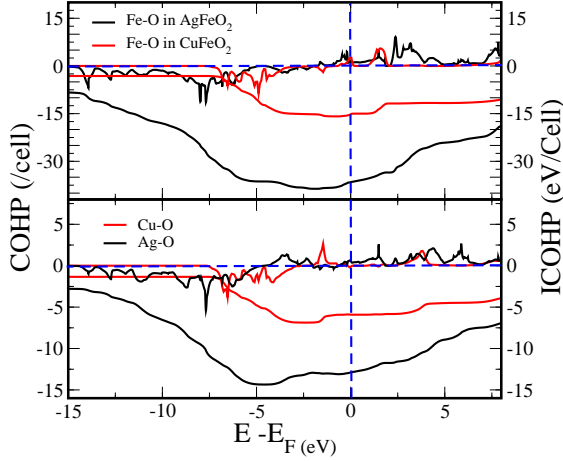


FIG. 4: (i) COHPs and integrated COHPs (ICOHP) per bond (a) for Fe-O for AgFeO₂ and CuFeO₂, and (b) Ag-O and Cu-O for AgFeO₂ and CuFeO₂ respectively.

tems (see Fig. 3), and also hybridize with the O-*p* states. For AgFeO₂, the Ag-4*d* states are completely filled and spread over -1 eV to -7 eV below the Fermi level (see Fig. 3(i)(c)). On the other hand for CuFeO₂, the Cu-3*d* states are completely filled and spread over -0.5 eV to -3 eV below the Fermi level (see Fig. 3(ii)(c)). Both the Ag-*d* and Cu-*d* states also hybridize with oxygens.

We have also compared the hybridization of Fe-O and also A-O (A = Cu, Ag) for these two systems by analyzing the COHP plots, that provide an energy resolved visualization of the chemical bonding. In COHP, the density of states is weighted by the Hamiltonian matrix elements where the off-site COHP represents the covalent contribution to bands. The bonding contribution for which the system undergoes a lowering in energy is indicated by negative COHP and the antibonding contribution that raises the energy is represented by positive COHP. Thus it gives a quantitative measure of bonding. In Fig. 4 we have plotted the off-site COHP and the energy integrated COHP (ICOHP) per bond for the nearest neighbor Fe-O and Ag-O for AgFeO₂ and Fe-O and Cu-O for CuFeO₂. From the COHP plots in Fig. 4, we find that strongest covalency is between Fe and O for both the systems. The Ag-O covalency is substantially stronger in comparison to

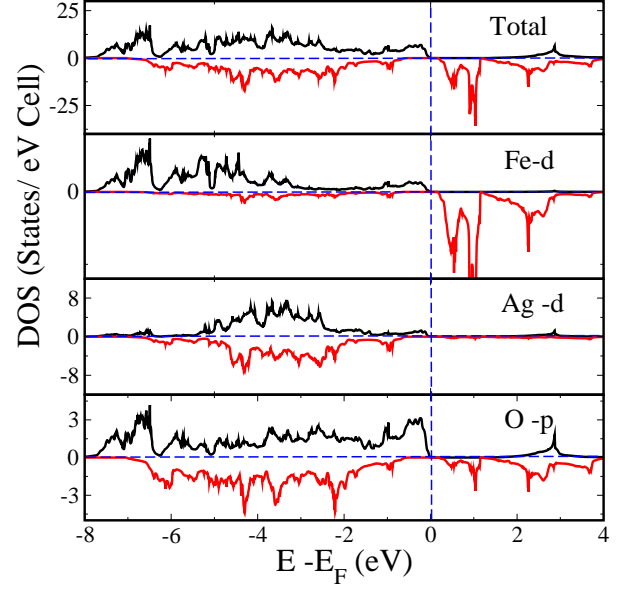


FIG. 5: Total and orbital decomposed density of states for AgFeO₂.

Cu-O covalency as revealed by the integrated COHP at the Fermi level where ICOHP value for Ag-O is -6.44 eV and for Cu-O, ICOHP value is -2.95 eV. Interestingly, the nearest-neighbor Fe-O covalency is larger for AgFeO₂ (ICOHP values are -6.092 and -2.53 eV for AgFeO₂ and CuFeO₂ respectively). This difference in hybridization with oxygen may be responsible for different magnetic ground state of AgFeO₂ and CuFeO₂.

2. Spin polarized calculations

In order to study the magnetic properties we have carried out spin-polarized calculations for AgFeO₂. The total and orbital decomposed density of states for ferromagnetic configurations are plotted in Fig. 5. As suggested in Ref. 28, we have used the onsite Coulomb interaction term $U = 3$ eV and the onsite exchange interaction $J = 1$ eV for Fe *d* states in AgFeO₂. From Fig. 5(a), we find that the ferromagnetic state is insulating with $U = 3$ eV and $J = 1$ eV in LSDA+*U* calculation. The plot of the density of states (DOS) reveal the presence of five electrons in Fe-3*d* spin up channel, which is consistent with the picture of high-spin Fe³⁺ ions in AgFeO₂. The O-*p* and Ag-*d* states are completely occupied. In ferromagnetic configuration, the spin moment of Fe site is $4.23 \mu_B$ with $U = 3$ eV and $J = 1$ eV, and the rest are partly accommodated in O ($m_O = 0.09 \mu_B$).

3. Symmetric exchange interactions

In order to determine the various exchange parameters (J_i), (indicated in Fig. 1(b)), we have first calculated the

TABLE I: Relative energies per three f.u (in meV) for AgFeO₂ determined from LSDA+U calculations.

Configuration	ΔE (for $U_{eff} = 2$ eV)	ΔE (for $U_{eff} = 4$ eV)
FM	0.0	0.0
AF1	-234.5	-99.54
AF2	-212.33	-94.03
AF3	-254.5	-111.57
AF4	-66.0	-31.4

TABLE II: Symmetric exchange interactions (in meV) for AgFeO₂ and CuFeO₂ are tabulated here. The exchange interactions for CuFeO₂ inside the parentheses, are adapted from Ref. 5.

Exchange	AgFeO ₂		CuFeO ₂
	$U_{eff} = 2$ eV	$U_{eff} = 4$ eV	$U_{eff} = 4$ eV
J_1	-1.92	-0.83	-0.77(-0.76)
J_2	-0.62	-0.21	-0.15(-.18)
J_3	-0.81	-0.35	-0.28(-.30)
J_4	-0.88	-0.42	-0.24(-.23)

total energies of several ordered spin states of a system and then related the energy differences between these states to the corresponding energy differences expected from the Heisenberg spin Hamiltonian:²⁹⁻³¹

$$H = \sum_{i,j} J_{ij} \vec{S}_i \cdot \vec{S}_j \quad (1)$$

We have calculated the total energies of five ordered spin states (FM, AF1, AF2, AF3, AF4) shown in Fig. 6. The total spin exchange energies (per three formula units) of the five ordered spin states are expressed as:

$$\begin{aligned}
 E(FM) &= \frac{25}{4}(-9J_1 - 9J_2 - 9J_3 - 9J_4) \\
 E(AF1) &= \frac{25}{4}(3J_1 + 3J_2 - 9J_3 - J_4) \\
 E(AF2) &= \frac{25}{4}(-J_1 + 3J_2 - J_3 - J_4) \\
 E(AF3) &= \frac{25}{4}(3J_1 - J_2 - J_3 - J_4) \\
 E(AF4) &= \frac{25}{4}(-9J_1 - 9J_2 - 9J_3 + 3J_4) \quad (2)
 \end{aligned}$$

The relative energies for AgFeO₂, calculated from LSDA+U method are summarized in Table I. The nearest neighbor, next-nearest-neighbor and diagonal interactions are denoted by J_1 , J_2 and J_3 respectively. J_4 denotes the coupling between nearest neighbors in adjacent layers. The exchange interactions are displayed in Table II. In last column of Table II, the values in the parentheses are the exchange interactions for CuFeO₂ obtained from Ref. 5. We find that all the exchange

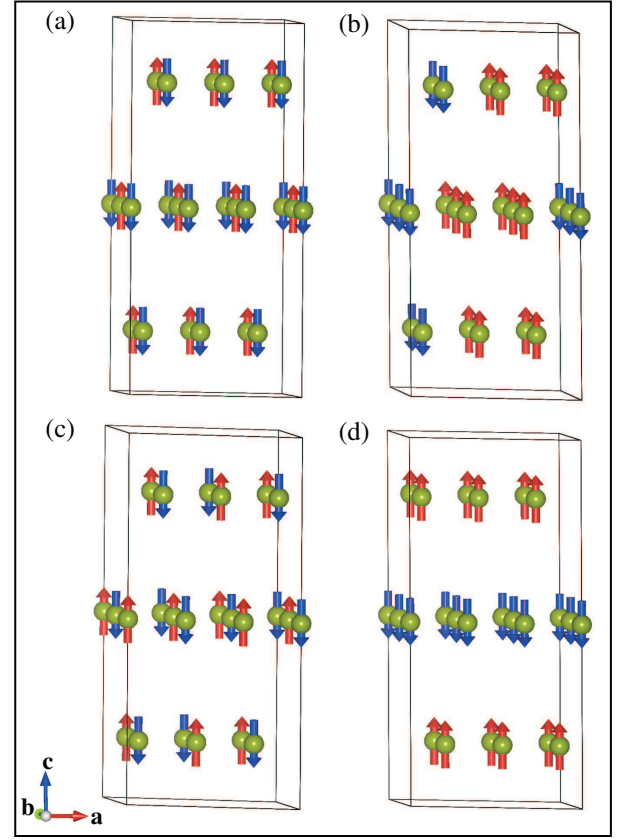


FIG. 6: The four ordered spin states (AF1, AF2, AF3, AF4) of AgFeO₂ constructed using a $(3 \times 2 \times 1)$ supercell. (a) AF1: spins are arranged ferromagnetically along a and c direction and antiferromagnetically along b direction, (b) AF2: the spin arrangement is $\uparrow\downarrow\downarrow$ along a direction and ferromagnetic along other two directions, (c) AF3: spins are antiferromagnetically arranged along a and b directions and ferromagnetically along c direction, (d) AF4: spin arrangement is such that intra-layer couplings are ferromagnetic and inter-layer couplings are antiferromagnetic.

interactions (J_1 , J_2 , J_3 , and J_4) are antiferromagnetic type. As a consequence both the intra-layer and the inter-layer exchange interactions are spin-frustrated in AgFeO₂ as well as in CuFeO₂. In AgFeO₂, the inter-layer exchange interaction J_4 is strongest in comparison to intra-layer exchange interactions J_2 and J_3 , while J_3 is dominant in CuFeO₂. The exchange interactions are of super exchange type for both the systems. The intra-plane J_1 exchange interaction is mediated by Fe-O-Fe super-exchange path. Other intra-plane exchange interactions J_2 and J_3 are mediated through Fe-O..O-Fe super exchange path. The inter planer exchange coupling J_4 is mediated via the Fe-O-A-O-Fe path. As we have shown by plotting COHP (see Fig. 4) that the hybridization of Ag with oxygen for AgFeO₂ is greater than the hybridization of Cu with oxygen for CuFeO₂, the inter layer coupling is much stronger for AgFeO₂. The antifer-

romagnetic nature of the exchange interactions in each FeO₂ layer results in spin frustration in the (J_1, J_1, J_1) and (J_2, J_2, J_2) triangles and in the (J_1, J_1, J_2) line segments. Between adjacent FeO₂ layers, spin frustration occurs in the isosceles (J_1, J_4, J_4) triangles. The silver ferrite appears to be a more frustrated system with higher values of exchange interaction parameters as compared to the copper ferrite. We have also calculated the Curie-Weiss temperature θ_{CW} for AgFeO₂. In the mean field limit, the Curie-Weiss temperature θ is related to the exchange interactions as follows:

$$\theta = \frac{S(S+1)}{3K_B} \sum_i z_i J_i \quad (3)$$

where, the summation runs over all nearest neighbors of a given spin site, z_i is the number of nearest neighbors connected by the spin exchange interaction J_i , and S is the spin quantum number of each spin site (i.e., $S = 5/2$ in the present case). The calculated Curie-Weiss temperature (θ_{CW}) for AgFeO₂ is -363 K and -252 K for $U_{eff} = 2$ and 4 eV respectively, while the experimental value is -140 K. Thus, according to the experimental Curie-Weiss temperature and the mean-field theory, the calculated J_1 - J_4 values are overestimated by a factor of $f = 2.6$ and 1.9 for $U_{eff} = 2$ and 4 eV respectively. The θ_{CW} for CuFeO₂ is -292 K with overestimation factor $f = 3.24$ as reported in Ref. 5. From the magnitude of the symmetric exchange interactions for AgFeO₂ and CuFeO₂, we conclude that the difference in the magnetic ground state for AgFeO₂ and CuFeO₂ probably do not stem from the symmetric part of the spin Hamiltonian. In the following, we have investigated the magnetic properties of AgFeO₂ and CuFeO₂ including spin orbit interaction.

4. Spin-orbit coupling

The importance of spin-orbit coupling in triangular lattice antiferromagnets has been discussed in literature.^{19,32} In this work we have investigated the importance of spin-orbit coupling and single ion anisotropy for AgFeO₂ and CuFeO₂. We have considered the FM spin configurations for both the system and included the spin orbit coupling (SOC) in the framework of LSDA+U+SOC calculations. The orbital moment at the Fe site is $\sim 0.028 \mu_B$ and $\sim 0.025 \mu_B$ for AgFeO₂ and CuFeO₂ respectively. For high spin configuration of Fe³⁺ ($3d^5$), the orbital moment is expected to be quenched. Here induced mechanism due to either mixing of Fe- d with oxygen p states or t_{2g} - e_g orbitals is possible leads to finite orbital moment. In fact, our COHP analysis suggests substantial hybridization between Fe and oxygen. We have calculated the total energy by choosing the various spin quantization axes, and the result of our calculation is displayed in Table III.^{33,34} An estimation of magnetocrystalline anisotropy is obtained from the energy difference between calculations with spin quantiza-

tion chosen along the c direction (001) and perpendicular to the c direction, yield values 0.33 meV and 0.21 meV per Fe ion for AgFeO₂ and CuFeO₂ respectively within LSDA+U+SOC (for $U_{eff} = 4$ eV) calculation. The magnetocrystalline anisotropy energy is larger for AgFeO₂ than CuFeO₂ indicating important role of SOC for AgFeO₂.

5. Antisymmetric exchange interactions

Next, we have considered the antisymmetric part of the spin Hamiltonian $H = \sum_{\langle ij \rangle} \vec{D}_{ij} \cdot (\vec{S}_i \times \vec{S}_j)$ and calculated the Dzyaloshinskii-Moriya interactions parameter (\vec{D}) from the total energy calculations with spin orbit coupling as discussed in Ref. 35. Here we have calculated the three components D_{12}^x , D_{12}^y , D_{12}^z of the DM vector (between nearest neighbor spin sites 1 and 2) for AgFeO₂ and CuFeO₂ by performing LSDA + U + SOC calculations. In order to calculate x component of \vec{D}_{12} , we consider the following four spin configurations in which the spins 1 and 2 are oriented along the y and z axes, respectively: (i) $S_1 = (0, S, 0)$, $S_2 = (0, 0, S)$, (ii) $S_1 = (0, -S, 0)$, $S_2 = (0, 0, S)$, (iii) $S_1 = (0, S, 0)$, $S_2 = (0, 0, -S)$, (iv) $S_1 = (0, -S, 0)$, $S_2 = (0, 0, -S)$. In these four spin configurations, the spins of all the other spin sites are the same and are along the x direction. The spin interaction energy for the four spin configurations can be written as

$$E_{spin} = E_{other} + D_{12}^x S_1^y S_2^z - S_1^y \sum_{i=3,4} D_{1i}^z S_i^x + S_2^z \sum_{i=3,4} D_{2i}^x S_i^y$$

Similarly for y and z components of \vec{D}_{12} . Our calculated values (in meV) of the components of \vec{D}_{12} for AgFeO₂ are $D_{12}^x = 0.0104$, $D_{12}^y = -0.42$ and $D_{12}^z = 0.005$ and the magnitude of DM vector is 0.4202 ($\frac{|D_{12}|}{J_1} = 0.55$) for $U_{eff} = 4$ eV. We have also computed \vec{D}_{12} for $U_{eff} = 2$ eV and corresponding components of \vec{D}_{12} are $D_{12}^x = 0.011$, $D_{12}^y = -0.87$, $D_{12}^z = 0.01$ and $\frac{|D_{12}|}{J_1} = 0.5$. The large y component of \vec{D}_{12} term makes the two spins perpendicular to each other in the ac -plane.^{36,37}

We have also calculated the components of \vec{D}_{12} (between nearest neighbor spin sites 1 and 2) for CuFeO₂. The components are $D_{12}^x = 0.004$, $D_{12}^y = -0.16$, $D_{12}^z = 0.012$ and the magnitude of DM vector is 0.161 ($\frac{|D_{12}|}{J_1} = 0.2$) for $U_{eff} = 4$ eV. For $U_{eff} = 2$ eV, the components are $D_{12}^x = 0.004$, $D_{12}^y = -0.23$, and $D_{12}^z = 0.012$ with $\frac{|D_{12}|}{J_1} = 0.15$. The DM vector for nearest neighbor sites, is much smaller for CuFeO₂ compared with AgFeO₂. These calculations suggest that SOC has a profound impact on AgFeO₂ and plays a key role in determining its magnetic ground state.

TABLE III: The energy differences between calculations with spin quantization chosen along different directions within LSDA+U+SOC calculations.

Quantized axis	ΔE for AgFeO ₂		ΔE for CuFeO ₂	
	$U_{eff} = 2$ eV	$U_{eff} = 4$ eV	$U_{eff} = 2$ eV	$U_{eff} = 4$ eV
(001)	0.0	0.0	0.0	0.0
(010)	0.83	0.33	0.65	0.21
(100)	0.83	0.33	0.65	0.21

6. Low temperature magnetic structure

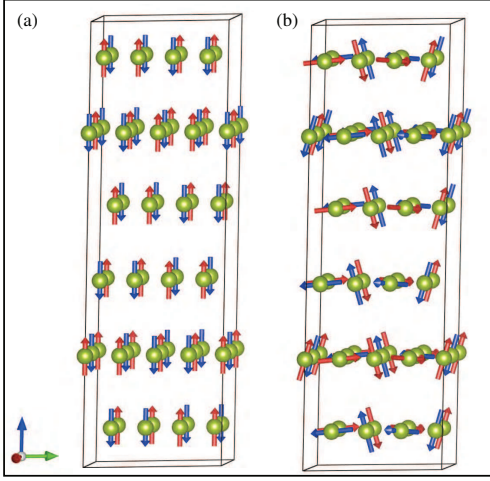


FIG. 7: (a) AFM1 collinear magnetic ordering (b) AFM2 noncollinear magnetic ordering.

In order to simulate the low temperature (below 9 K) magnetic order of AgFeO₂, we have made a (2×4×2) supercell which contains 192 atoms. We have considered two magnetic configurations AFM1 and AFM2 as shown in Fig. 7. In AFM1 configuration ($q = (\frac{1}{2}, \frac{1}{4}, \frac{1}{2})$) the spin arrangement along b direction is $\uparrow\uparrow\downarrow\downarrow$ and they are antiferromagnetically aligned along a and c direction. For AFM2 configuration ($q = (\frac{1}{2}, \frac{1}{4}, \frac{1}{2})$), we have made the noncollinear spin arrangements along b directions. Spins are antiferromagnetically aligned along a and c directions. The three components of spin at Fe sites for a Fe-O layer is displayed in Table IV.

We have calculated the electronic structure for the FM, AFM1, and AFM2 using LSDA+U method. The results of our calculations are displayed in Table V and we find that the AFM1 magnetic configuration has the lowest in energy. The total and partial density of states in the AFM1 magnetic configuration for AgFeO₂ calculated using LSDA+U method, is shown in Fig. 8. The band gap in AFM1 state is calculated to be 0.54 eV and 1.03 eV for $U_{eff} = 2$ and 4 eV respectively. The majority Fe- d states are completely occupied while the minority states are empty, which is consistent with the Fe³⁺ valence state of Fe with a $3d^5$ configuration. Such a half-filled config-

TABLE IV: The three components of spin (in μ_B) for one Fe-O layer in AFM2 magnetic configuration for AgFeO₂ determined from LSDA+U calculations ($U_{eff} = 2$ eV).

m_x	m_y	m_z
-0.822	2.690	3.090
0.801	-2.600	-3.152
3.038	2.872	0.012
0.128	2.801	-3.100
-3.027	2.875	-0.215
-0.165	-0.363	4.157
-3.046	-2.845	-0.228
3.055	-2.845	0.019

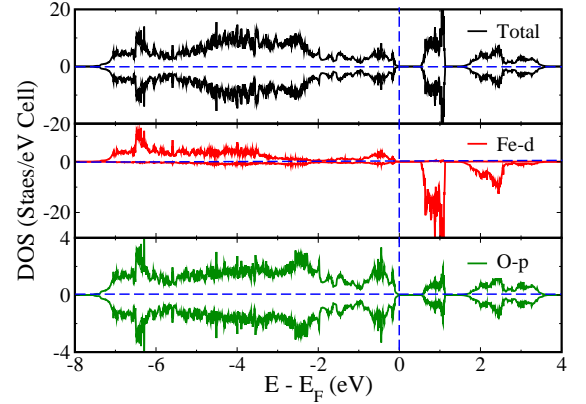


FIG. 8: The plot of total and orbital projected density of states in AFM1 magnetic configuration for AgFeO₂ within LSDA+U calculation (for $U_{eff} = 2$ eV).

uration promotes the antiferromagnetic order. The spin magnetic moment of Fe is $3.982 \mu_B$ and $4.18 \mu_B$ with $U_{eff} = 2$ and 4 eV respectively.

We have added the spin orbit coupling (SOC) in our calculation. The results of our calculation for AFM1 and AFM2 structures is displayed in Table V. Our calculations clearly reveal AFM2 is the ground state for AgFeO₂ upon inclusion of SOC, indicating important role of spin orbit interaction as anticipated earlier. The spin and orbital moments at Fe sites are $4.15 \mu_B$ and $0.027 \mu_B$ respectively.

TABLE V: The relative energies (in meV) for AFM1, AFM2, and FM magnetic configurations within LSDA+U and LSDA+U+SOC calculations.

Configurations	LSDA+U	LSDA+U+SOC
AFM1	-24	76
AFM2	0.0	0.0
FM	43	86

TABLE VI: The bond length between the magnetic atoms in experimental structure and change in bond length in relaxed structures. (change in bond length -Ve means the shortening of bond length after relaxation)

Exchange paths	Distance (Å) Exp. Struc.	change in bond length (Å) (AFM1 relax)	change in bond length (Å) (AFM2 relax)
J_1	3.09	-0.04	-0.09
J_2	5.26	0.01	0.06
J_3	6.08	-0.01	0.02
J_4	6.44	0.0	0.01

B. Ferroelectric properties

Finally, we have calculated the ferroelectric polarization with AFM1 and AFM2 magnetic configuration using Berry phase method²⁷ as implemented in the VASP.²⁴ We do not find the electric polarization for the centrosymmetric crystal structure with AFM1 and AFM2 magnetic structure within LSDA+U for $U_{eff} = 2$ eV. With the application of spin orbit coupling (SOC), there is no polarization for AFM1 structure, however AFM2 magnetic configuration attains a polarization value of $34 \mu C/m^2$ respectively, which suggests that the non-collinear magnetic order induces polarization via spin orbit coupling. Therefore spin-current mechanism is one source of the electric polarization in this system. But our calculated magnitude of electric polarization is much smaller than the observed experimental value of polarization ($\sim 300 \mu C/m^2$ for powder sample). This result suggests that although there is electronic contribution to the polarization but the lattice mechanism also important for the ferroelectric polarization in $AgFeO_2$.

In order to obtain the lattice contribution to polarization, we have carried out relaxation calculations within the framework of LSDA+U and LSDA+U+SOC method. In this optimization, the cell parameters were fixed to the experimental values, but the positions of the atoms were allowed to relax. The maximum change in bond lengths occurs for the nearest neighbor. The bond lengths before and after relaxations are listed in Table VI. The ferroelectric polarization of $282 \mu C/m^2$ is found for the relaxed AFM1 collinear structure without SOC. This result sug-

TABLE VII: Calculated Polarization ($\mu C/m^2$) in various magnetic structures

Structure	P ($U_{eff}=2$ eV)	P ($U_{eff}=4$ eV)
Exp. AFM1	0	0
Exp. AFM2	0	0
Exp. AFM2 + SOC	34	26
Relax. AFM1	282	264
Relax. AFM1 + SOC	324	308
Relax. AFM2	407	373
Relax. AFM2 + SOC	485	453

gests that symmetric spin exchange induces the polarization in this material through the exchange-striction mechanism. Application of SOC, the polarization turn out to be $324 \mu C/m^2$. The polarization is increased for relaxed AFM2 noncollinear structure, and the value of polarization is $407 \mu C/m^2$ with $U_{eff} = 2$ eV in LSDA+U calculation without SOC. We find that the polarization in relaxed structure with AFM2 magnetic configuration with spin-orbit coupling is $485 \mu C/m^2$. We have also calculated the electric polarization with a larger value of U . Our results are summarized in Table VII. Our results suggest that the exchange striction mechanism as well as spin current model¹² are responsible for electric polarization in this system.

III. CONCLUSION

In this paper, we have studied the electronic structure, magnetism, and ferroelectric properties of the triangular lattice antiferromagnet $AgFeO_2$ and compared our results with isostructural compound $CuFeO_2$. While Fe is in d^5 configuration in both the systems, the magnetic ground state of $AgFeO_2$ markedly different from $CuFeO_2$. In order to understand the origin of this difference, we calculated the symmetric exchange interactions offered by the Heisenberg model. Our calculations reveal that the symmetric exchange interactions are nearly identical for both the systems and therefore hardly play any role for the different magnetic ground state. Next, we incorporated spin-orbit coupling and our calculations regarding the orbital moment, magneto-crystalline anisotropy and DM parameters clearly indicate that SOC has a profound effect on $AgFeO_2$. It is interesting to note that SOC is operative in Fe $3d^5$ manifold possibly by induced mechanism due to either mixing of Fe- d with oxygen p states or mixing of $t_{2g} - e_g$ orbitals in the distorted octahedra. We recover the experimental magnetic ground state of $AgFeO_2$ upon the inclusion of SOC. Calculations of ferroelectric polarization suggest that the spontaneous polarization arises from noncollinear spin arrangement via spin-orbit coupling. Our calculations also indicate that in addition to electronic contributions, lattice me-

diated contribution to the polarization is also important for AgFeO_2 .

-
- * Present address: Department of Physics, Indian Institute of Science Education and Research Bhopal, Bhauri, Bhopal 462066, India
- ¹ L. Balents, *Nature* **464**, 199 (2010).
 - ² G. Lawes, M. Kenzelmann, N. Rogado, K. H. Kim, G. A. Jorge, R. J. Cava, A. Aharony, O. Entin-Wohlman, A. B. Harris, T. Yildirim, Q. Z. Huang, S. Park, C. Broholm, and A. P. Ramirez, *Phys. Rev. Lett.* **93**, 247201 (2004).
 - ³ B. Koteswararao, R. Kumar, J. Chakraborty, B.-G. Jeon, A. V. Mahajan, I. Dasgupta, K. H. Kim, and F. C. Chou, *J. Phys.: Condens. matter* **25**, 336003 (2013).
 - ⁴ K. Kimura, H. Nakamura, S. Kimura, M. Hagiwara, and T. Kimura, *Phys. Rev. Lett.* **103**, 107201 (2009).
 - ⁵ Y. Zhang, E. Kan, and M.-h. Whangbo, *Chem. Mater.* **23**, 4181 (2011).
 - ⁶ S. Seki, Y. Onose, and Y. Tokura, *Phys. Rev. Lett.* **101**, 067204 (2008).
 - ⁷ A. Vasiliev, O. Volkova, I. Presniakov, A. Baranov, G. Demazeau, J.-M. Broto, M. Millot, N. Leps, R. Klingeler, B. Büchner, M. B. Stone, and A. Zheludev, *J. Phys.: Condens. matter* **22**, 016007 (2010).
 - ⁸ M. Malvestuto, F. Bondino, E. Magnano, T. T. a. Lumen, P. H. M. van Loosdrecht, and F. Parmigiani, *Phys. Rev. B* **83**, 134422 (2011).
 - ⁹ S. Mitsuda, H. Yoshizawa, N. Yaguchi, and M. Mekata, *J. Phys. Soc. Jpn.* **60**, 1885 (1991).
 - ¹⁰ O. A. Petrenko, G. Balakrishnan, M. R. Lees, D. McK. Paul, and A. Hoser, *Phys. Rev. B* **62**, 8983 (2000).
 - ¹¹ M. Mekata, N. Yaguchi, T. Takagi, T. Sugino, S. Mitsuda, H. Yoshizawa, N. Hosoi, and T. Shinjo, *J. Phys. Soc. Jpn.* **62**, 4474 (1993).
 - ¹² H. Katsura, N. Nagaosa, and A. V. Balatsky, *Phys. Rev. Lett.* **95**, 057205 (2005).
 - ¹³ N. A. Spaldin and M. Fiebig, *Science* **309**, 391 (2005).
 - ¹⁴ D. I. Khomskii, *J. Magn. Magn. Mater.* **306**, 1 (2006).
 - ¹⁵ J. Chakraborty, N. Ganguli, T. Saha-dasgupta, and I. Dasgupta, *Phys. Rev. B* **88**, 094409 (2013).
 - ¹⁶ T. Arima, *J. Phys. Soc. Jpn.* **76**, 073702 (2007).
 - ¹⁷ M. Soda, K. Kimura, T. Kimura, M. Matsuura, and K. Hirota, *J. Phys. Soc. Jpn.* **78**, 124703 (2009).
 - ¹⁸ E. J. Kan, H. Xiang, Y. Zhang, C. Lee, and M.-H. Whangbo, *Phys. Rev. B* **80**, 104417 (2009).
 - ¹⁹ N. Terada, D. Khalyavin, P. Manuel, Y. Tsujimoto, K. Knight, P. Radaelli, H. Suzuki, and H. Kitazawa, *Phys. Rev. Lett.* **109**, 097203 (2012).
 - ²⁰ S. Okamoto, I. Okamoto, and T. Ito, *Acta Crystallogr.* **28**, 1774 (1972).
 - ²¹ N. Terada, D. D. Khalyavin, P. Manuel, Y. Tsujimoto, and A. A. Belik, *Phys. Rev. B* **91**, 094434 (2015).
 - ²² R. D. Shannon and a. D. B. R. Charles T. Prewitt, *Inorg. Chem.* **10**, 719 (1971).
 - ²³ P. E. Blöchl, *Phys. Rev. B* **50**, 17953 (1994).
 - ²⁴ G. Kresse and J. Furthmüller, *Phys. Rev. B* **54**, 11169 (1996).
 - ²⁵ O. K. Andersen and O. Jepsen, *Phys. Rev. Lett.* **53**, 2571 (1984).
 - ²⁶ S. L. Dudarev, G. A. Botton, S. Y. Savrasov, C. J. Humphreys, and A. P. Sutton, *Phys. Rev. B* **57**, 1505 (1998).
 - ²⁷ R. Resta, *Rev. Mod. Phys.* **66**, 899 (1994).
 - ²⁸ K. P. Ong, K. Bai, P. Blaha, and P. Wu, *Chem. Mater.* **2**, 634 (2007).
 - ²⁹ H. J. Xiang, C. Lee, and M. H. Whangbo, *Phys. Rev. B* **76**, 220411(R) (2007).
 - ³⁰ J. Chakraborty and I. Dasgupta, *Phys. Rev. B* **86**, 054434 (2012).
 - ³¹ B. Koteswararao, A. V. Mahajan, F. Bert, P. Mendels, J. Chakraborty, V. Singh, I. Dasgupta, S. Rayaprol, V. Siruguri, a. Hoser, and S. D. Kaushik, *J. Phys.: Condens. Matter* **24**, 236001 (2012).
 - ³² Y. Tanaka, N. Terada, T. Nakajima, M. Taguchi, T. Kojima, Y. Takata, S. Mitsuda, M. Oura, Y. Senba, H. Ohashi, and S. Shin, *Phys. Rev. Lett.* **109**, 127205 (2012).
 - ³³ J. Chakraborty, S. Samanta, B. R. K. Nanda, and I. Dasgupta, *J. Phys.: Condens. Matter* **28**, 375501 (2016).
 - ³⁴ J. Chakraborty, *J. Phys.: Condens. Matter* **29**, 395801 (2017).
 - ³⁵ H. Xiang, E. Kan, S.-H. Wei, M.-H. Whangbo, and X. Gong, *Phys. Rev. B* **84**, 224429 (2011).
 - ³⁶ X. Z. Lu, M.-H. Whangbo, S. Dong, X. G. Gong, and H. J. Xiang, *Phys. Rev. Lett.* **108**, 187204 (2012).
 - ³⁷ Z.-L. Li, M.-H. Whangbo, X. G. Gong, and H. J. Xiang, *Phys. Rev. B* **86**, 174401 (2012).